

# An instrumented tracer for Lagrangian measurements in Rayleigh-Bénard convection

Woodrow L. Shew, Yoann Gasteuil, Mathieu Gibert, Pascal Metz & Jean-François Pinton

*Laboratoire de Physique de l'École Normale Supérieure de Lyon, CNRS UMR5672,*

*46 allée d'Italie F-69007 Lyon, France*

## Abstract

We have developed novel instrumentation for making Lagrangian measurements of temperature in diverse fluid flows. A small neutrally buoyant capsule is equipped with on-board electronics which measure temperature and transmit the data via a wireless radio frequency link to a desktop computer. The device has 80 dB dynamic range, resolving milli-Kelvin changes in temperature with up to 100 ms sampling time. The capabilities of these “smart particles” are demonstrated in turbulent thermal convection in water. We measure temperature variations as the particle is advected by the convective motion, and analyse its statistics. Additional use of cameras allow us to track the particle position and to report here the first direct measurement of Lagrangian heat flux transfer in Rayleigh-Bénard convection. The device shows promise for opening new research in a broad variety of fluid systems.

PACS numbers: 47.80.-v (Instrumentation for fluid flows); 44.27.+g (Convective heat transfer)

## I. INTRODUCTION

Scalar mixing in turbulent flows plays a crucial role in uncountable natural, medical, and industrial systems: spread of pollutants by wind and water; oceanic and atmospheric thermal convection; the life cycles of plankton; mixing in combustion engines and chemical reactors. A natural approach to understanding these examples is to measure the trajectories of the pollutant molecules, warm fluid elements, planktonic organisms, and chemical species, respectively, as well as the properties of the flow along these trajectories. This Lagrangian approach to turbulent mixing has been advanced significantly with numerical and theoretical models [1], but experimental works are rare due to the difficulties in (1) distinguishing the identity of a fluid particle along its trajectory, and (2) making measurements along these paths. A few recent experimental studies have successfully performed resolved measurements of the trajectories of small solid tracer particles in turbulence [2, 3, 4, 5]. Atmospheric research groups [6] and oceanographers routinely employ meter-sized Lagrangian floats to study large scale flows [7]. Lagrangian probes have a distinct advantage over Eulerian probes which record at fixed positions in the flow: the measurements provide information about local physical processes as experienced by the fluid particle.

With the aim of measuring Lagrangian scalar quantities in well-controlled laboratory flows, we have developed a miniature, wireless, neutrally-buoyant instrument, dubbed a *smart particle*. We present temperature measurements obtained with this device in turbulent thermal convection. Similar instruments have been used in medical applications [8], but to our knowledge we report the first such measurement device in the context of fluid dynamics. Simultaneous measurements of temperature and position have been made before in convection experiments, most recently by tracking optically the motion of microspheres containing thermochromic liquid crystal (TLC) [9]. The shape evolution of thermal plumes very close to the thermal and hydrodynamic boundary layers was quantified, but this method is not capable of tracking individual particles over large distances. Our smart particle measurements complement those of TLC particles by vastly improving temperature and time resolution as well as allowing observation of very long particle trajectories, though the smart particles are too large to investigate the flow in the boundary layers.

## II. DEVICE DETAILS

The details of the instrument are describe in the following five subsections. First we present a block diagram and general description of the whole system. Then, the radio frequency (RF) data transfer is described in detail. Next, we focus on the power management system. We then discuss the measurement and processing of temperature data and end with details about the position measurement technique.

### A. Overview

The smart particle consists of a  $D = 21$  mm diameter capsule containing temperature instrumentation, an RF emitter, a battery, and an on-off switch – illustrated in Figs. 1(a,b). A resistance controlled oscillator is used to create a square wave whose frequency depends on the temperature of several thermistors. This square wave is used directly to modulate the amplitude of the radio wave generated by the RF emitter. The entire mobile circuit is powered with a coin cell battery and may be put in a low power standby mode using an externally applied magnetic field.

The stationary parts of the system include an antenna, an RF receiver, 2 RF amplifiers, a high speed data acquisition system, and a desktop computer running Labview (Fig. 1a). The broad-band radio frequency amplifiers increase the voltage amplitude of the signal by a factor of 26 dB. The receiver is carefully tuned to demodulate the signal produced by the emitter. The receiver outputs a square wave identical to that generated by the resistance controlled oscillator. The frequency of this square wave, and hence temperature, is recovered on-the-fly using a Labview algorithm. In addition, the particle trajectory is recorded with a digital video camera, resulting in synchronous measurements of the position and temperature of the particle as it is carried about by the fluid.

### B. RF data link

The radio frequency emitter is a MAX7044 (from Maxim Integrated Products), which employs on-off keying (OOK) amplitude modulation. The RF carrier frequency is 315 MHz. The MAX7044 expects a digital modulating signal with a baud rate from 0 to 100 kHz. We implement an 8 mm diameter, 8-turn coil emitter antenna with about 200 nH inductance

and 4  $\Omega$  resistance. We use a split-capacitor impedance matching network to maximize the efficiency since the MAX7044 is optimized for a 125  $\Omega$  antenna. The emitter draws an average of 5 mA and requires 2.1-3.6 V from the battery in normal operation. The emitter consumes 10 to 100 times more power than any of the other on-board components.

On the receiving end we use the MAX1473 superheterodyne receiver, which demodulates OOK data and is designed to work with the MAX7044. The receiving antenna is a 315 MHz 1/4 wave whip (Linx Technologies, Inc., ANT-315-CW-HD). Between the antenna and the receiver are two low noise amplifiers each with a gain of 13 dB at 315 MHz (MAX2640).

### C. Power management

The size of the instrumentation capsule is minimized so that it capable of probing as small a spatial scale as possible. The component of the system which limits the size of the capsule most is the battery. It is a CR1616 lithium coin cell (Panasonic), which is 16 mm in diameter and 1.6 mm thick. This battery can supply the necessary power for about 3 hours. The circuit is also equipped with a magnetic field triggered switch so that the instrumentation may be turned off when we are not ready to acquire data. The switch is composed of a TLE4913 low power hall switch (Infineon Technologies) and a NL17SZ74 single D flip-flop (ON Semiconductor). The hall switch outputs a high logic level when in the presence of a sufficiently large magnetic field. Feeding this output into the CP pin of the flip-flop while D is connected to  $\bar{Q}$  we have a “push-button” switch, which is operable with a hand-held permanent magnet from a distance of several centimeters. When the switch is in the “off” position, the circuit consumes less than 100  $\mu$ A. The hall switch and the flip-flop respectively require 2.4-5.5 V and 1.65-5.5 V from the battery.

### D. Temperature detection

The system measures the spatially averaged temperature around the smart particle body. This is accomplished using four thermistors to set the frequency of a LMC555 timer/oscillator (National Semiconductor) operating in astable mode. The thermistors protrude from the capsule wall by about 0.5 mm and are spaced evenly around its middle. The LMC555 outputs a square wave at logic levels with a period  $1/f = (R_1 + R_2 + 2R_3 +$

$2R_4)C/1.44$ , where  $R_i$  are the resistances of the four thermistors, and  $C$  is 47 pF. We employ 0.8 mm, 230 k $\Omega$  thermistors (Epcos B57540G0234) with a response time of about 0.06 s in water, which is faster than the fastest temperature time scales of the flow we study. In the range of temperature 26 – 34 °C, the frequency of the square wave is in the range 22 – 26 kHz; the sensitivity is 513 Hz/°C. The relationship between temperature and frequency is linear within 2 percent. The LMC555 requires about 100  $\mu$ A at a supply voltage between 1.5 and 12 V.

The RF receiver recovers the square wave signal, which is then recorded with a high-speed, 14 bit, analog-to-digital converter (ADC) (National Instruments 5621 in a PXI system). Running on a desktop PC, Labview is used to control the data acquisition. The frequency of the demodulated square wave is computed on-the-fly using a standard Labview library. Each measurement of frequency is computed from 100 ms of the square wave, i.e. about 3000 periods, sampled by the ADC at 10 MHz. The resulting measurement resolution is about  $\pm 2$  Hz, which is  $\pm 4$  mK when converted to temperature. The sampling rate is about 10 Hz. With maximum flow velocities in the range 1-2 cm/s and a particle size of 21  $\mu$ m, we are oversampling the dynamics by a factor of order 10.

### E. Position measurement

In order to measure the smart particle position, we use a standard webcam, interfaced with a desktop computer. A uniform well-illuminated image background is achieved with a back-lit sheet of frosted glass. We use Matlab scripts to control the camera and process the video data. First, each video frame is converted into a 2D binary array, using an adaptive threshold. Then, the particle position is extracted using an image recognition algorithm. The effective sample frequency is around 5 Hz. The resolution of the camera is 640  $\times$  480 pixels, so that the particle position is determined with 0.1 mm precision.

## III. MEASUREMENTS IN RAYLEIGH-BÉNARD CONVECTION

### A. Convection apparatus

Our experimental setup, shown in figure 1c, is a traditional rectangular Rayleigh-Bénard cell with height  $H = 40$  cm and section 40 cm  $\times$  10 cm. The fluid is water and the walls of

the vessel are 25 mm thick PMMA. The upper plate of the cell is temperature regulated by a chilled water bath. The bottom plate is heated by 5 resistors, regularly spaced. Complete experimental details can be found in [10].

In the results reported here, the power input is  $P = 230$  W, and the upper plate is regulated to  $T_{\text{up}} = 19^\circ\text{C}$ , corresponding to a temperature difference between the top and bottom plates of  $\Delta T = 20.3^\circ\text{C}$ . As a result, the Rayleigh number is

$$Ra = \frac{g\beta\Delta TH^3}{\nu\kappa} = 3.07 \times 10^{10}, \quad (1)$$

where  $g$  is acceleration due to gravity,  $\beta = 2.95 \times 10^{-4} \text{ K}^{-1}$  is the thermal expansion coefficient of water and  $\nu = 8.17 \times 10^{-7} \text{ m}^2\text{s}^{-1}$ ,  $\kappa = 1.48 \times 10^{-7} \text{ m}^2\text{s}^{-1}$  its viscosity and thermal diffusivity (values are given for a mean temperature equal to  $29.1^\circ\text{C}$ ). The Nusselt number, measured as the total heat flux normalized by  $\kappa\Delta T/L$ , is  $Nu = 167.9 \pm 0.2$ . Under these conditions, the convective regime is fully turbulent [10, 13] and the mean flow is a steady, system-sized, single convection roll with a rotation period of about 100 s. The characteristic thickness of the thermal boundary layer is  $\ell_T \sim \frac{1}{2}HNu^{-1} \sim 1.2$  mm and that of the hydrodynamic boundary layer is  $\ell_U \sim \ell_T(\nu/\kappa)^{1/3} \sim 2$  mm. Thus, the particle is too large to penetrate the boundary layers.

## B. Temperature measurement

The particle and fluid density are carefully matched. This is achieved by initially adjusting the particle mass to within 1 percent of  $\rho_f\pi D^3/6$ , where  $\rho_f$  is the density of water. Then, to obtain neutral buoyancy within 0.05 percent,  $\rho_f$  is finely adjusted by the addition of small amounts (about 1000 ppm) of pure glycerol, which has a density 20 percent greater than water. The particle is inevitably slightly lighter than the cool fluid near the upper plate and slightly heavier than the warm fluid near the bottom plate. Nonetheless, the particle explores all regions of the vessel without a clear bias as can be seen in figure 2b.

We show in figure 3a, a time series of the temperature  $\theta(t)$  recorded by the particle, during the trajectory shown in figures 2b,c. Apparent in the time series is a nearly periodic, large amplitude fluctuation, which reflects the particle's entrainment in the mean flow. This periodicity, as well as the smaller amplitude turbulent fluctuations are made more clear in the power spectrum shown in figure 3b. The spectrum also reveals a range of time scales,

corresponding to frequencies  $0.016 < f < 0.230$  Hz, which is consistent with a self-similar  $\tilde{\theta}^2 \sim f^{-\alpha}$  scaling, with an exponent  $\alpha$  close to -2. This feature is in sharp contrast with the Eulerian temperature spectrum obtained when the particle is constrained to remain at fixed location in space. In that case, we have verified that the spectrum shows an  $f^{-7/5}$  scaling range. This value is in agreement with other experimental Eulerian studies of convection (e.g. [11]), provided the frequency spectrum be interpreted as a spectrum in space, which is plausible considering the persistent mean flow (i.e. Taylor’s hypothesis). Bolgiano-Obhukov scaling also leads to a  $k^{-7/5}$  wavenumber spectrum for temperature variations in real space. By contrast, the spectral behavior found here for the moving particle is reminiscent of velocity data for Lagrangian tracers in turbulent flows. Indeed when fluid turbulence is fully developed, a well-established feature of Lagrangian dynamics and Kolmogorov’s theory is that the Lagrangian velocity spectrum should have an  $f^{-2}$  inertial range [3, 12] – as we have verified also verified here from our independent measurement of the particle position. The upper cut-off frequency apparent in figure 3b around ( $\sim 0.3$  Hz) corresponds to the characteristic time of motion of the particle across a distance equal to its diameter  $D$ : the mean speed of the large scale roll being  $\approx 1.6$   $\text{cm s}^{-1}$ . This is also in agreement with Lagrangian measurements made using density matched tracers: the velocity spectrum was found to follow the expected Lagrangian behavior up to a frequency set by the particle’s size and the flow characteristic velocity scale [3]. These interpretations are consistent with qualitative observations using Schlieren visualization, which reveal that temperature plumes of size  $D$  or larger fully entrain the smart particle, while smaller plumes do so only partially.

Finally, as shown in figure 3c, the histogram of temperature is non-Gaussian. The non-Gaussian character of the PDF is in agreement with Eulerian measurements using fixed temperature probes [13]. Other recent experimental studies have also shown that the distribution of intense temperature plumes in the form of mushrooms has non Gaussian tails [9]. We note that the asymmetry of the PDF is probably due to imperfect density matching between the fluid and the particle, so that it tends to stay slightly longer near the bottom plate.

### C. Heat flux measurement

With the assumption that the particle may indeed act as a Lagrangian tracer in the convective flow, it is natural and interesting to discuss the heat carried by the flow in terms of the temperature measured by the particle. To this end, we define an instantaneous Lagrangian Nusselt number as:

$$Nu^L(t) = 1 + \frac{L}{\kappa\Delta T}\theta'(t) \cdot v_z(t) , \quad (2)$$

where  $\theta'(t) = \theta(t) - \bar{\theta}$  is the particle temperature variation from its time averaged temperature  $\bar{\theta}$ , and  $v_z(t)$  its vertical velocity. Integrating this quantity over all the fluid particles in any horizontal plane recovers the traditional Nusselt number.

The time series of  $Nu^L$  is shown in figure 4a. Comparing this time series with the trajectory in figure 2(c), we see that the heat transfer intermittently spikes to very large values often as the particle moves away from the end plates and mixes with fluid at intermediate heights in the vessel. The power spectrum in figure 4b shows that the periodicity of the large scale convection roll is diminished and strong fluctuations occur over a broader range of (slow) scales. The spectrum shows a fast,  $f^{-4}$  decrease in the same frequency range that the temperature showed  $f^{-2}$ . As discussed in the previous section, this scaling is consistent with our understanding of velocity spectra ( $\tilde{v}^2 \sim f^{-2}$ ) resulting in  $\tilde{Nu}^{L^2} \sim \tilde{\theta}^2 \tilde{v}^2 \sim f^{-4}$ . The PDF of  $Nu^L$ , figure 4c is skewed toward positive values, as expected because coherent convective motion are associated with either hot fluid rising or cold fluid sinking, so that in each case  $\theta' \cdot v_z > 0$ . The much less probable events with  $\theta' \cdot v_z < 0$  correspond, for instance, to the rise of the particle when it is colder than its environment. This is unlikely but not impossible as the particle may be trapped in the swirls of a turbulent plume (e.g. the flow in the “cap” of the mushroom shaped plume is opposite the flow in the “stem”). The most probable value of the PDF is zero, indicating the particle spends a large amount of time at the mean fluid temperature in the bulk of the cell. The mean value,  $\overline{Nu^L}$ , is more surprising: at 335.4 it is roughly twice the global, Eulerian, Nusselt value computed from power input and velocity differences. Such an increased mean may be due to the fact that the particle does not sample the flow uniformly, but may instead get more advection from intense thermal plumes. The dramatically non-Gaussian form of the PDF as well as scale-by-scale statistics of the local flux requires further study. This analysis will be reported elsewhere.



## IV. CONCLUSIONS

We report on new instrumentation for making fluid mechanics measurements in the reference frame of particles passively advected by flow motion. These smart particles show promise for a fresh perspective in turbulence research as well as two phase flows. The rapid development of MEMS and microfluidic components, which may be incorporated in a smart particle, opens a diverse range of potential applications including granular flows and reacting flows in chemical and biological systems.

We demonstrate the capabilities of smart particles in the simple case of Lagrangian temperature measurements in thermal convection. We report several original findings. First, we observe  $f^{-2}$  power law scaling behavior for the temperature spectrum, which suggests the temperature acts as a passive scalar advected by fully developed, Kolmogorov-like, turbulence. This result supports the hypothesis that outside the boundary layers, where buoyancy sets the fluid into motion, the temperature is passively mixed in the turbulent bulk. (e.g. [14, 15, 16]). Strong temporal intermittency in Lagrangian heat transport is revealed in the extremely heavy-tailed probability distribution functions, while the fact that the mean Lagrangian heat transport is much higher than the Eulerian average suggests strong spatial inhomogeneity as well. Further and deeper investigations of these features will be presented soon elsewhere.

### Acknowledgements

The authors have had fruitful discussions with Francesca Chillá and Bernard Castaing. This work has been supported by C.N.R.S. and Emergence Contract No. 2005-12 from the French Rhône-Alpes Region.

- 
- [1] G. Falkovich, K. Gawedzki, M. Vergassola, *Rev. Mod. Phys.* **73**, 913 (2001)
  - [2] S. Ott, J. Mann, *J. Fluid Mech.*, **422** 207 (2000)
  - [3] N. Mordant et al. *Phys. Rev. Lett.*, **87**(21), 214501, (2001)  
N. Mordant, P. Metz, O. Michel, J.-F. Pinton, *Rev. Sci. Instr.* **76** 025105 (2005)
  - [4] La Porta A.L., et al., *Nature*, 409, 1017, (2001)  
H. Xu et al. *Phys. Rev. Lett.* **96**, 024503 (2006)

- M. Bourgoïn, N. T. Ouellette, H. Xu, J. Berg & E. Bodenschatz, *Science* **311**, 835 (2006).
- [5] B. Luthi, A. Tsinober, W. Kinzelbach, *J. Fluid Mech.* **528**, 87 (2005)
- [6] F. Gifford, *Month. Weather Rev.* **83**(12), 293 (1955) S. Hanna, *J. Appl. Meteo.* **20**, 242 (1981)
- [7] R.-C. Lien, E.A. D'Asaro, G.T. Dairiki, *J. Fluid Mech.* **362**, 177 (1998)
- [8] S. Mackay, B. Jacobson, *Nature* **179**, 1239 (1957)  
R. H. Colson et al. *Biotelem. Pat. Mon.* **8**, 213 (1981).
- [9] Q. Zhou, C. Sun, K.-Q. Xia, *Phys. Rev. Lett.* **98**, 074501 (2007)
- [10] F Chillá et al., *Nouvo Cimento* **15**, 1229 (1993).  
M. Gibert et al. *Phys. Rev. Lett.* **96**, 084501 (2006).
- [11] J. A. Glazier, T. Segawa, A. Naert and M. Sano, *Nature* **398**, 307 (1999)  
X. Z. Wu, L. Kadanoff, A. Libchaber, and M. Sano, *Phys. Rev. Lett.* **64**, 2140 (1990).
- [12] P.K. Yeung, *An. Rev. Fluid Mech.* **34**, 115 (2002)  
N. Mordant, E. Lévêque, J.-F. Pinton, *New J. Phys.* **6**, 116 (2004)  
L. Biferale et al. *Phys. Fluids* **17**, 021701 (2005)
- [13] B. Castaing et al., *J. Fluid Mech.* **204**, 1 (1989).
- [14] S. Sun, Q. Zhou, K.-Q. Xia, *Phys. Rev. Lett* **97**, 144504 (2006).
- [15] B. I. Shraiman and E. D. Siggia, *Phys. Rev. A* **42**, 3650 (1990).
- [16] B. Castaing, *Phys. Rev. Lett.* **65**, 3209 (1990).

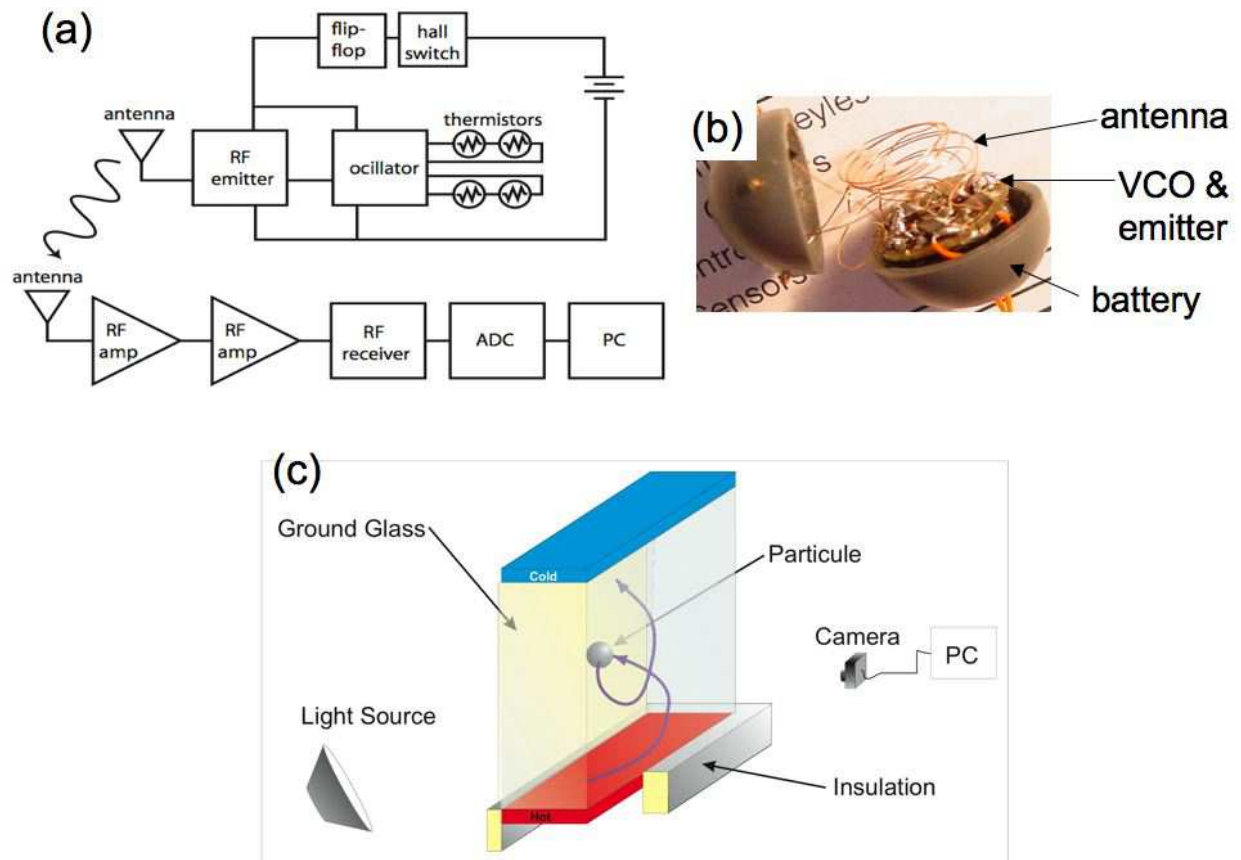


FIG. 1: (a) Block diagram of measurement system. (b) Photo of the smart particle before closing the capsule.

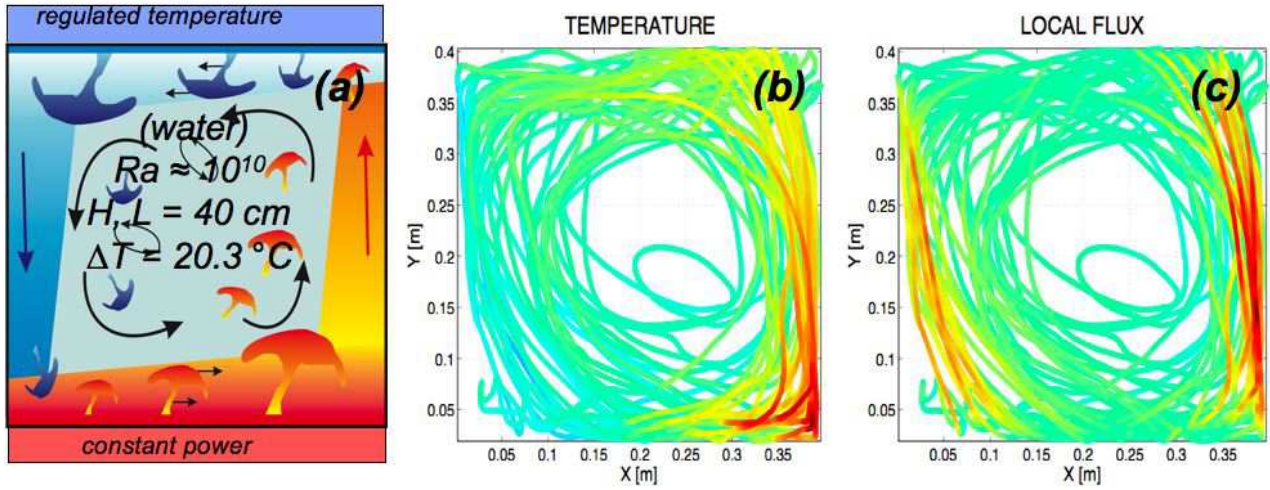


FIG. 2: (a) Cartoon of the convection flow. The black disc represents the smart particle. (b,c) Trajectory of the particle with temperature (b) and heat flux (c) encoded in the color.

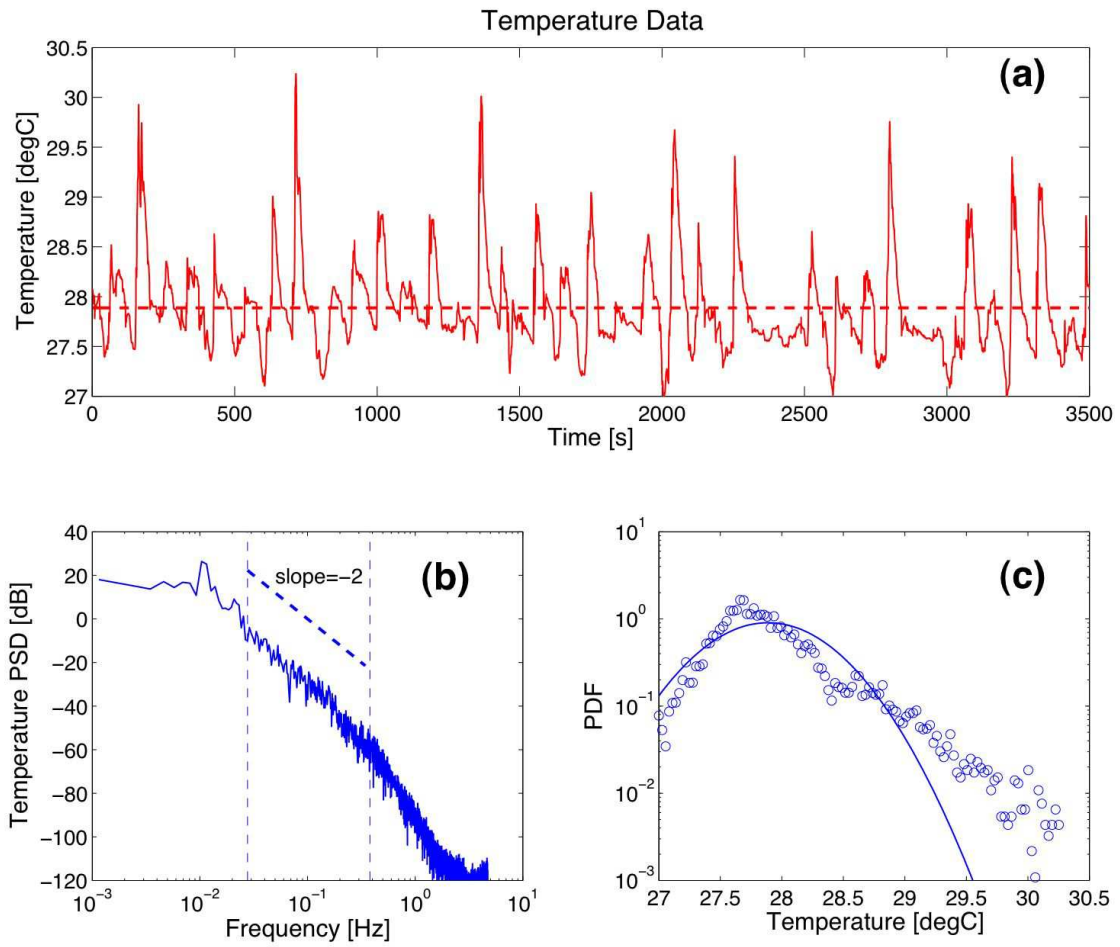


FIG. 3: Temperature measurements: (a) time series for the trajectory in figure 2(a). The mean temperature is 27.887 degC and the standard deviation is 0.451 degC; (b) corresponding power spectrum; (c) Temperature probability density function (circles), compared to a Gaussian (solid line).

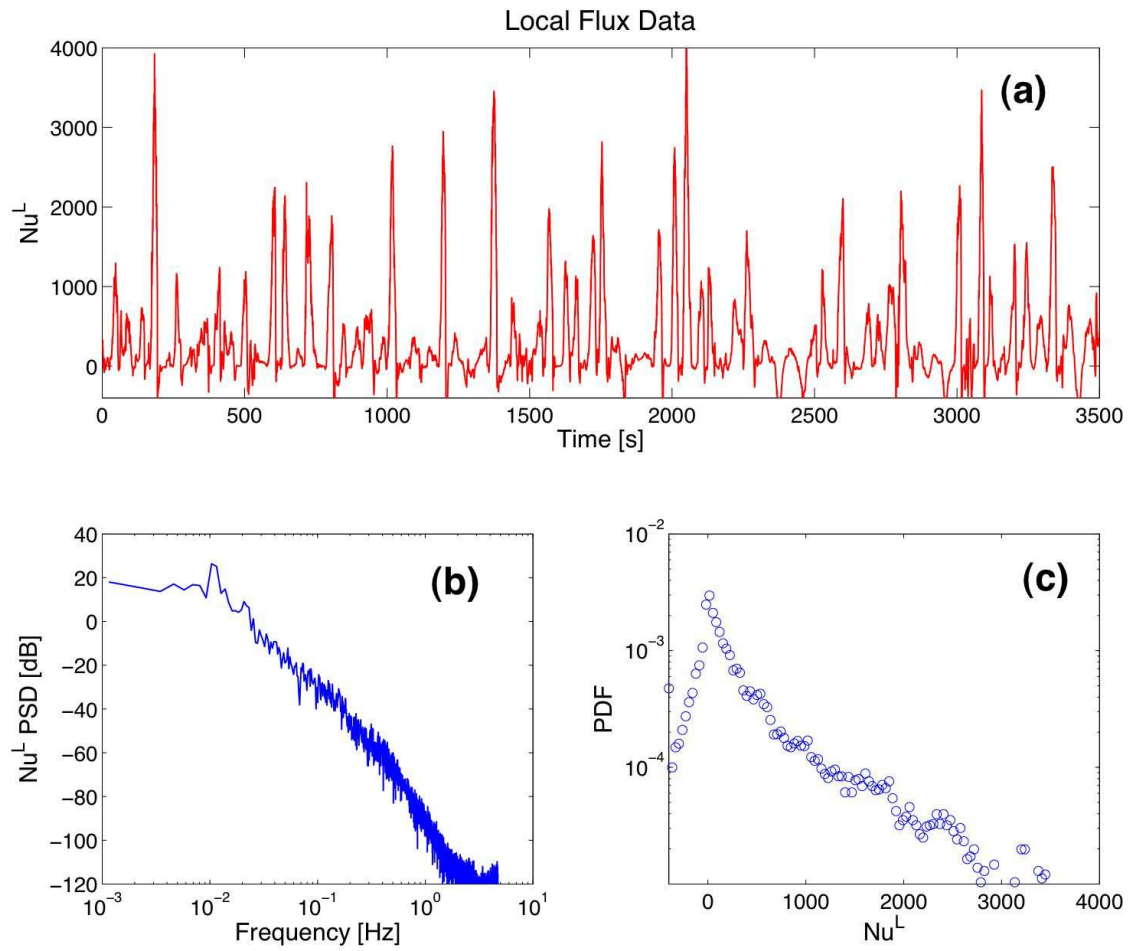


FIG. 4: Heat flux measurements: (a) time series of  $Nu^L(t)$  for the trajectory in figure 2(a); (b) corresponding power spectrum; (c) Probability density function.